nature physics

LETTERS

https://doi.org/10.1038/s41567-018-0250-5

# Direct entropy measurement in a mesoscopic quantum system

Nikolaus Hartman[1,2*], Christian Olsen[1,2], Silvia Lüscher[1,2], Mohammad Samani[1,2,3,9], Saeed Fallahi[4,5,6], Geoffrey C. Gardner[5,6,7], Michael Manfra[4,5,6,7,8] and Joshua Folk[1,2*]

**The entropy of an electronic system offers important insights into the nature of its quantum mechanical ground state. This is particularly valuable in cases where the state is difficult to identify by conventional experimental probes, such as conductance. Traditionally, entropy measurements are based on bulk properties, such as heat capacity, that are easily observed in macroscopic samples but are unmeasurably small in systems that consist of only a few particles[1,2]. Here, we develop a mesoscopic circuit to directly measure the entropy of just a few electrons, and demonstrate its efficacy using the well-understood spin statistics of the first, second and third electron ground states in a GaAs quantum dot[3–8]. The precision of this technique, quantifying the entropy of a single spin-1/2 to within 5% of the expected value of $k_B \ln 2$, shows its potential for probing more exotic systems. For example, entangled states or those with non-Abelian statistics could be clearly distinguished by their low-temperature entropy[9–13].**

Our approach is analogous to the milestone of spin-to-charge conversion achieved over a decade ago, in which the infinitesimal magnetic moments of a single spin were detected by transforming them into the presence or absence of an electron charge[14,15]. Following this example, we perform an entropy-to-charge conversion, making use of the Maxwell relation

$$\left(\frac{\partial \mu}{\partial T}\right)_{p,N} = -\left(\frac{\partial S}{\partial N}\right)_{p,T} \quad (1)$$

that connects changes in entropy, particle number and temperature ($S$, $N$ and $T$, respectively) to changes in the chemical potential, $\mu$, a quantity that is simple to measure and control. The condition of fixed pressure, $p$, in equation (1) is met by working well below the Fermi temperature of the reservoir, $T_F \sim 100\,\mathrm{K}$, where degeneracy pressure dominates[16].

The Maxwell relation in equation (1) forms the basis of two theoretical proposals to measure non-Abelian exchange of Moore–Read quasiparticles in the $\nu = 5/2$ state via their entropy[9,10]. Ref. [10] proposes a strategy by which quasiparticle entropy could be deduced from the temperature-dependent shift of charging events on a local disorder potential—a thermodynamic equivalent of the measurements that established the $e/4$ quasiparticle charge at $\nu = 5/2$ (ref. [17]). As a demonstration of the viability and the high accuracy achievable by this technique, we investigate a well-understood system with localized fermions in place of more exotic quasiparticles: a few-electron GaAs quantum dot. The entropies of the first three electron states in the dot are measured by the temperature-dependent charging scheme laid out in ref. [10]. Applying the language of quantum dots to equation (1), the entropy difference between the $N-1$ and $N$ electron ground states ($\Delta S_{N-1\to N}$ for $\Delta N = 1$) is measured via the shift with temperature in the electrochemical potential, $\mu_N$, needed to add the $N$th electron to the dot.

The measurement relies on the mesoscopic circuit shown in Fig. 1a, using electrostatic gates to realize an electron reservoir in thermal and diffusive equilibrium with a few-electron quantum dot coupled to its right side. The occupation of the dot is tuned with the plunger gate voltage, $V_p$, and measured using an adjacent quantum point contact as a charge sensor[18–20]. Applying more positive $V_p$ lowers $\mu_N$, bringing the $N$th electron into the dot when $\mu_N$ drops below the Fermi level of the reservoir, $E_F$. The reservoir temperature, $T$, can be increased above the GaAs substrate temperature by Joule heating from current, $I_{heat}$, driven through a quantum point contact on the left side. Charge transitions on the dot appear as steps in the charge sensor conductance, $G_{sens}(V_p)$, thermally broadened by the reservoir temperature (Fig. 1b,c). The gate voltage corresponding to the midpoint of the transition, $V_{mid}$, marks the electrochemical potential at which the probabilities of finding $N-1$ and $N$ electrons on the dot are equal.

When $\mu_N$ shifts with temperature, $V_{mid}$ also shifts; it is the shift in $V_{mid}$ with temperature that forms the basis of our experiment (Fig. 1c). In practice, charge noise limits the accuracy to which $V_{mid}$ can be measured. To overcome this, the measurement is done with a lock-in amplifier, oscillating the temperature using an a.c. $I_{heat}$ and measuring resultant oscillations in $G_{sens}$, which we label $\delta G_{sens}$. As seen in the insets of Fig. 1b,c, the lineshape of $\delta G_{sens}$ is perfectly antisymmetric when $\partial S/\partial N = 0$, but asymmetric when $\partial S/\partial N \neq 0$.

The temperature-induced shift in the dot chemical potential with respect to the reservoir $E_F$ can also be understood in terms of detailed balance. At $V_{mid}$, where probabilities for $N$ and $N-1$ electrons on the dot are equal, the tunnel rates $\Gamma_{in} = \Gamma_{N-1\to N}$ and $\Gamma_{out} = \Gamma_{N\to N-1}$ must also be equal. These rates depend on the number of available states in the tunnelling process, and therefore on the degeneracies, $d_{N-1}$ and $d_N$, of the $N-1$ and $N$ ground states[21,22]. The condition $\Gamma_{in} = \Gamma_{out}$ leads to a simple relationship between degeneracy and the thermally broadened Fermi function, $f(\mu_N - E_F, T)$:

[1]Stewart Blusson Quantum Matter Institute, University of British Columbia, Vancouver, British Columbia, Canada. [2]Department of Physics and Astronomy, University of British Columbia, Vancouver, British Columbia, Canada. [3]Fields Institute for Research in Mathematical Sciences, Toronto, Ontario, Canada. [4]Department of Physics and Astronomy, Purdue University, West Lafayette, IN, USA. [5]Station Q Purdue, Purdue University, West Lafayette, IN, USA. [6]Birck Nanotechnology Center, Purdue University, West Lafayette, IN, USA. [7]School of Materials Engineering, Purdue University, West Lafayette, IN, USA. [8]School of Electrical and Computer Engineering, Purdue University, West Lafayette, IN, USA. [9]Present address: The Hospital for Sick Children, Toronto, Ontario, Canada. *e-mail: nik.hartman@gmail.com; jfolk@physics.ubc.ca

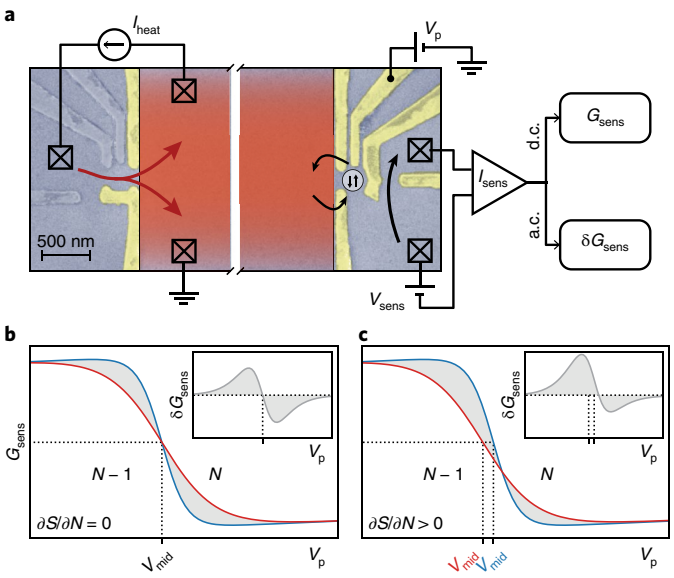


**Fig. 1 | Measurement protocol. a**, A scanning electron micrograph of a device similar to the one measured. Electrostatic gates (gold) define the circuit in a two-dimensional electron gas (2DEG), with grey gates grounded. The squares indicate ohmic contacts to the 2DEG. The temperature of the electron reservoir in the middle (red) is oscillated using a.c. current, $I_{heat}$, at frequency $f_{heat}$ through the quantum point contact (QPC) on the left. A portion of the 5-μm-wide reservoir has been removed here for clarity. The occupation of the quantum dot, tunnel coupled to the right side of the reservoir, is tuned by $V_p$ and monitored by $I_{sens}$ through the charge sensor QPC. $I_{sens}$ is split into d.c. and a.c. components, the latter being measured by a lock-in amplifier at $2f_{heat}$. **b**,**c**, Simulated d.c. charge sensor signal, $G_{sens}$, for a transition from $N-1 \rightarrow N$ electrons at two temperatures ($T_{Red} > T_{Blue}$), showing two possible cases for $\frac{\partial S}{\partial N}$. The insets show the corresponding difference, $\delta G_{sens}$, between hot and cold curves.

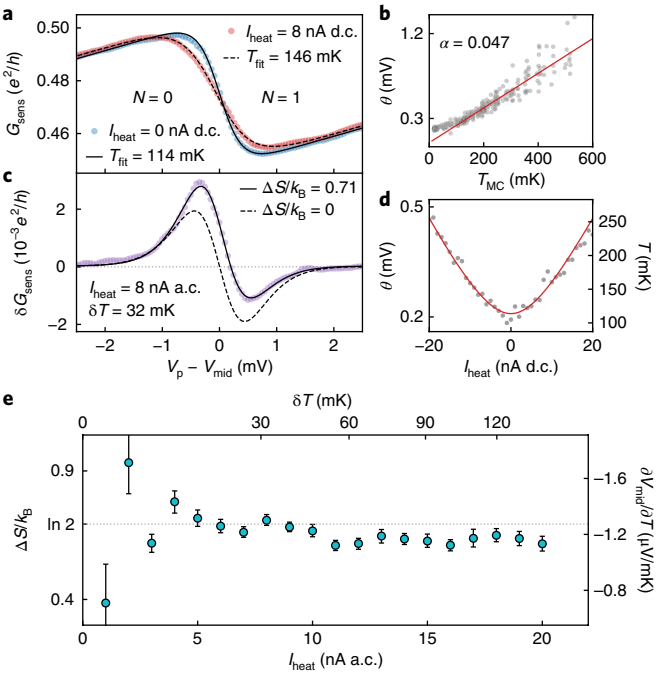


**Fig. 2 | Entropy measurement for a single spin-1/2. a**, Charge sensor data for $N=0 \rightarrow 1$ at two temperatures set by d.c. current through the QPC heater. **b**, The transition width, $\Theta$, was linear in $T_{MC}$ above 100 mK, for $I_{heat}=0$. The lever arm $\alpha$ is calculated by fitting a straight line to this region. **c**, Lock-in measurement of $\delta G_{sens}$ with $\delta T = 32$ mK, determined from the calibration in **d**. Fits to $\delta G_{sens}$ (equation (3)) are shown with $\Delta S/k_B$ as a free parameter (solid) and fixed at $\Delta S/k_B = 0$ (dashed). **d**, $\Theta$ grows with d.c. current through the QPC heater. A fit to $T^2 = aT_{MC}^2 + bI_{heat}^2 R_{QPC}$ is used to convert between $I_{heat}$ and $\delta T$, where $T_{MC}$ is the mixing chamber temperature[30]. **e**, Entropy measurements were independent of the magnitude of $I_{heat}$ oscillations over a large range. The top axis indicates the corresponding magnitude of $\delta T$, while the right axis shows the entropy signal converted to a gate voltage shift per unit temperature. The error bars show 95% confidence intervals calculated with the bootstrap method.

$d_{N-1}/d_N = f/(1-f)$. Using the Boltzmann entropy, $S_N = k_B \ln d_N$, this relationship becomes $\Delta S_{N-1\rightarrow N} = (\mu_N - E_F)/T$, clearly demonstrating the connection between entropy, temperature and the shift in $\mu_N$ at $V_{mid}$. Previous experiments have explored the relationship between tunnel rates and degeneracy using time-resolved transport spectroscopy and by coupling quantum dots to atomic force cantilever oscillations[8,23–25]. The approach presented here is a thermodynamic analogue, and extends entropy measurements to a wider set of applications where tunnelling processes may not be observable in real time.

The dot was tuned such that the source was weakly tunnel-coupled to the reservoir with the drain closed. The conductance of the charge sensor was tuned to $G_{sens} \sim e^2/h$, where it was most sensitive to charge on the dot. The addition of the first electron to the dot was marked by a decrease in $G_{sens}$ that is consistent with a thermally broadened two-level transition (Fig. 2a):

$$G_{sens}(V_p, \Theta) = G_0 \tanh\left(\frac{V_p - V_{mid}(\Theta)}{2\Theta}\right) + \gamma_1 V_p + G_2 \qquad (2)$$

where $G_0$ quantifies the sensor sensitivity, $\Theta = \frac{k_B T}{\alpha e}$ is the thermal broadening expressed in units of gate voltage, $\alpha = \frac{1}{e}\frac{d\mu_N}{dV_p}$ is the lever arm, $\gamma_1$ reflects the cross-capacitance between the charge sensor and plunger gate, and $G_2$ is an offset. Figure 2a shows two such transition curves with thermal broadening set by $I_{heat}$. For $I_{heat}=0$, $\Theta$ followed $T_{MC}$ down to approximately 100 mK (Fig. 2b), validating the approximation of thermal broadening used throughout this experiment.

The data in Fig. 2c, and the corresponding fits, illustrate a measurement of $\Delta S_{0\rightarrow 1}$ across the $0 \rightarrow 1$ electron transition. The lock-in measurement of $\delta G_{sens}$, due to temperature oscillations $\delta T$, yields the characteristic peak–dip structure seen in Fig. 2c. The expected lineshape of such a curve is $\delta G_{sens} = \frac{\partial G_{sens}}{\partial T}\delta T$, with $G_{sens}$ defined by equation (3). This lineshape depends explicitly on $\Delta S$, recognizing (via equation (1)) that $\frac{\partial V_{mid}}{\partial \Theta} = \frac{1}{k_B}\frac{\partial \mu}{\partial T} = -\frac{1}{k_B}\Delta S_{N-1\rightarrow N}$:

$$\delta G_{sens}(V_p, \Theta) \propto -\delta T\left[\frac{V_p - V_{mid}(\Theta)}{2\Theta} - \frac{\Delta S}{2k_B}\right]\cosh^{-2}\left(\frac{V_p - V_{mid}(\Theta)}{2\Theta}\right) + \text{const.} \qquad (3)$$

As expected from Fig. 1b,c, $\delta G_{sens}(V_p)$ is antisymmetric around $V_{mid}$ for $\Delta S = 0$, and asymmetric for $\Delta S \neq 0$. A fit of the data in Fig. 2c to equation (3) yields $\Delta S_{0\rightarrow 1} = (1.02 \pm 0.03) k_B \ln 2$, closely matching the expected $\Delta S_{0\rightarrow 1} = S_1 - S_0 = k_B \ln 2$ for transitions between an empty dot with zero entropy ($S_0 = 0$) and the two-fold degenerate one-electron state ($d_1 = 2$) with entropy $S_1 = k_B \ln 2$.

It is important to note that $\Delta S$ is extracted from fits to equation (3) based solely on the asymmetry of the lineshape, with no calibration of measurement parameters (such as $\delta T$ or the lever

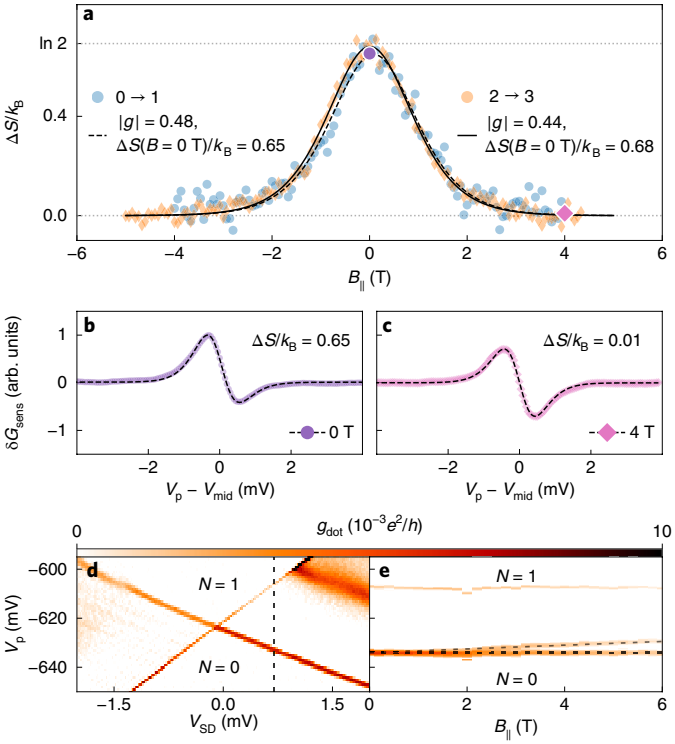


**Fig. 3 | Magnetic field dependence. a**, Changes in entropy for $N=0\rightarrow1$ and $2\rightarrow3$ transitions, overlaid to highlight similar behaviours. Each data point corresponds to a single $\delta G_{sens}(V_p)$ fit; multiple scans are carried out at various in-plane magnetic fields. **b**,**c**, Characteristic $\delta G_{sens}$ traces from which the data in **a** were extracted. The two data points corresponding to **b**,**c** are shown as large markers in **a**. **d**, Bias spectroscopy data for the $N=0\rightarrow1$ transition. The dashed line at $V_{SD}=700\,\mu$eV shows where data in **e** are taken. **e**, Fixed-bias data showing fits to Zeeman splitting of the ground state (dashed lines) from which $|g|=0.42\pm0.01$ is extracted.

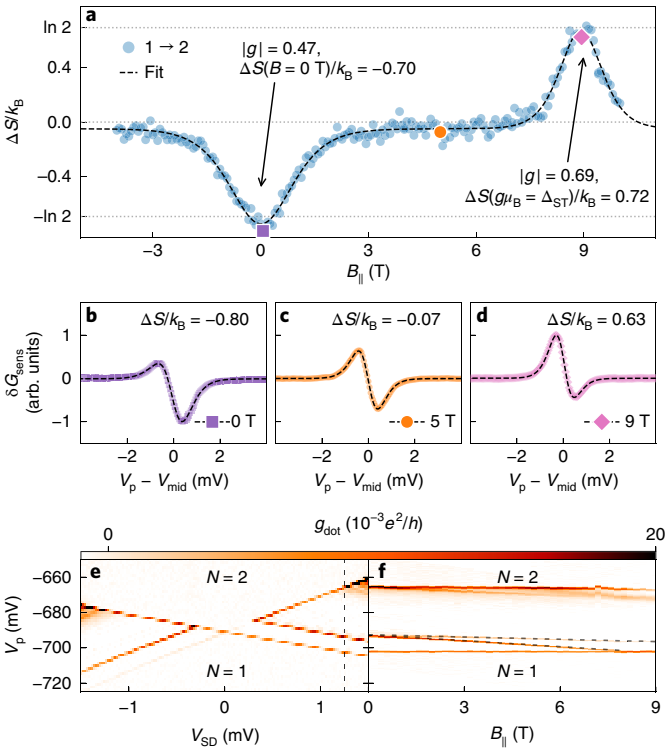


**Fig. 4 | Entropic signature of a singlet–triplet crossing. a**, Change in entropy, $\Delta S_{1\rightarrow2}$, extracted from $\delta G_{sens}$ fits at varying in-plane field. The dashed line shows a fit to equation (4), allowing for an offset from $\Delta S=0$ away from the degenerate points to compensate for nonlinearities in the charge sensor. The values stated for $\Delta S$ are with respect to the vertical offset apparent in the data. **b**–**d**, Characteristic $\delta G_{sens}$ traces from which the data in **a** were extracted. These data points are shown as large markers in **a**. **e**, Bias spectroscopy data for the $N=1\rightarrow2$ transition. Transitions to the two-electron triplet state correspond to the lines appearing at $V_{SD}=\pm320\,\mu$eV. The dashed line at $V_{SD}=1{,}250\,\mu$eV shows where the data in **f** are taken. **f**, Fixed-bias data in the in-plane field. The triplet level is split into $|\mathcal{T}_+\rangle$ and $|\mathcal{T}_0\rangle$ levels with a third $|\mathcal{T}_-\rangle$ level not visible here. At 8.4 T, $|\mathcal{T}_+\rangle$ becomes degenerate with $|\mathcal{S}\rangle$. $|g|=0.40\pm0.04$ is determined using $|\mathcal{T}_0\rangle$ and $|\mathcal{T}_+\rangle$ fits (dashed).

arm $\alpha$) required. We can, however, estimate $\alpha$ and $\delta T$ by determining $\Theta$ from fits to equation (2) for varying substrate temperature (Fig. 2b) and $I_{heat}$ (Fig. 2d). Measurements of $\Delta S$ remained constant over a broad range of $\delta T$ (Fig. 2e), as expected for temperatures low enough not to excite orbital degrees of freedom on the dot.

Confirmation that the measured $\Delta S$ derives from spin degeneracy is seen through its evolution with in-plane magnetic field, $B_{||}$. Figure 3a compares $\Delta S(B_{||})$ for the $0\rightarrow1$ and $2\rightarrow3$ transitions, both of which correspond to transitions from total spin zero to total spin one-half. The entropies of the one- and three-electron states go to zero as Zeeman splitting lifts the spin degeneracy, following the Gibbs entropy for a two-level system:

$$S=k_B\sum_{i=\pm}p_i(B_{||},T)\ln p_i(B_{||},T) \tag{4}$$

where

$$p_\pm(B_{||},T)=\left(1+e^{\mp\frac{g\mu_B B_{||}}{k_B T}}\right)^{-1} \tag{5}$$

are the probabilities for the unpaired electron to be in the spin-up or spin-down states at a given field and temperature. Fits to equation (4), with the ratio $g/T$ and an added scaling $\Delta S(B=0)$ as free parameters, give $\Delta S_{0\rightarrow1}(B=0)=(0.94\pm0.03)k_B\ln2$ and $\Delta S_{2\rightarrow3}(B=0)=(0.98\pm0.02)k_B\ln2$ (Fig. 3), and reflect the collapse to zero at high field where spin degeneracy is broken. This collapse can also be seen qualitatively, in the crossover from asymmetric to antisymmetric lineshapes of $\delta G_{sens}(V_p)$ (Fig. 3b,c). Estimating an average $T$ for each data set using the calibration in Fig. 2d yields $|g|=0.48\pm0.02$ and $|g|=0.44\pm0.01$ for the $0\rightarrow1$ and $2\rightarrow3$ transitions, respectively. The errors in the $g$-factor measurement are likely to be due to the difficulty of estimating temperature oscillations. Still, the $g$-factors are consistent with reported values[26–28] and the value measured separately in Fig. 3e using bias spectroscopy.

The $1\rightarrow2$ transition can be understood as the inverse of the $0\rightarrow1$ transition for $B_{||}<5$ T, comparing Figs. 3a and 4a. For relatively low fields, the two-electron ground state remains a spin singlet with zero entropy, while the one-electron entropy goes from $k_B\ln2$ to 0 due to Zeeman splitting. At higher fields, the one-electron ground state remains non-degenerate while the two-electron ground state gains a two-fold degeneracy when the singlet $|\mathcal{S}\rangle$ and triplet $|\mathcal{T}_+\rangle$ states cross. This singlet-triplet crossing is seen in bias spectroscopy data (Fig. 4f) at 8.4 T, and in the appearance of a peak in $\Delta S_{1\rightarrow2}$ at 9 T (Fig. 4a). The discrepancy in field required to drive the singlet–triplet degeneracy in Fig. 4a,f is attributed to a change in shape of

the dot potential, caused by altering the confinement gate voltages, when transitioning from one to two open tunnel barriers.

The field-dependent entropy measurement for the $1 \rightarrow 2$ transition can again be fitted using equation (4), with probabilities in equation (5) for the one-electron states and

$$\begin{aligned} p_{|\mathcal{S}\rangle}(B_{||},T) &= \left(1+\mathrm{e}^{-\frac{g\mu_B B_{||}-\Delta_{\mathcal{ST}}}{k_B T}}\right)^{-1} \\ p_{|\mathcal{T}_+\rangle}(B_{||},T) &= \left(1+\mathrm{e}^{+\frac{g\mu_B B_{||}-\Delta_{\mathcal{ST}}}{k_B T}}\right)^{-1} \end{aligned} \quad (6)$$

for the two-electron states, where $\Delta_{\mathcal{ST}}$ is the singlet–triplet splitting at zero field. From the fit, we find $\Delta S_{1\rightarrow 2}$ at the two-fold degenerate points, $B=0$ and 9 T, are $-(1.01\pm0.03)k_B \ln 2$ and $(1.04\pm0.04)k_B \ln 2$, respectively. The extracted $g$-factor, $|g|=0.47\pm0.02$, from the peak at $B=0$ is consistent with the $0\rightarrow 1$ transition. Around the high-field singlet–triplet degeneracy, we find $|g|=0.69\pm0.04$, an unexpectedly high $g$-factor that is explained by a shift of the $|\mathcal{T}_0\rangle$ state with magnetic field, as seen in Fig. 4f and previous work[29].

We conclude with a few notes to encourage the application of this entropy measurement protocol to other mesoscopic systems. The crucial ingredients in achieving the high accuracy reported here were: the ability to oscillate temperature rapidly enough to avoid $1/f$ noise; the ability to measure charging transitions without perturbing the localized states; and the fact that the charging transitions were thermally broadened. The last criterion enabled the entropy determination purely by asymmetry, without the need to know $\delta T$ or other measurement parameters accurately, yielding an uncertainty of less than 5%. With this level of precision, it should be possible, for example, to distinguish the $\frac{1}{2}k_B \ln 2$ entropy of a non-Abelian Majorana bound state from the $k_B \ln 2$ entropy of an Andreev bound state at an accidental degeneracy[11,12]. Similarly, the $S=\frac{1}{2}k_B \ln 2$ two-channel Kondo state could be clearly distinguished from fully screened ($S=0$) or unscreened ($S=k_B \ln 2$) spin states[13].

## Methods

Methods, including statements of data availability and any associated accession codes and references, are available at https://doi.org/10.1038/s41567-018-0250-5.

Received: 3 April 2018; Accepted: 12 July 2018;
Published online: 20 August 2018

## References

1. Ramirez, A. P., Hayashi, A., Cava, R. J., Siddharthan, R. & Shastry, B. S. Zero-point entropy in spin ice. *Nature* **399**, 333–335 (1999).
2. Schmidt, B. A. et al. Specific heat and entropy of fractional quantum Hall states in the second Landau level. *Phys. Rev. B* **95**, 201306 (2017).
3. Tarucha, S., Austing, D. G., Honda, T., van der Hage, R. J. & Kouwenhoven, L. P. Shell filling and spin effects in a few electron quantum dot. *Phys. Rev. Lett.* **77**, 3613–3616 (1996).
4. Ciorga, M. et al. Addition spectrum of a lateral dot from Coulomb and spin-blockade spectroscopy. *Phys. Rev. B* **61**, R16315–R16318 (2000).
5. Duncan, D. S., Goldhaber-Gordon, D., Westervelt, R. M., Maranowski, K. D. & Gossard, A. C. Coulomb-blockade spectroscopy on a small quantum dot in a parallel magnetic field. *Appl. Phys. Lett.* **77**, 2183–2185 (2000).
6. Lindemann, S. et al. Stability of spin states in quantum dots. *Phys. Rev. B* **66**, 195314 (2002).
7. Potok, R. M. et al. Spin and polarized current from Coulomb blockaded quantum dots. *Phys. Rev. Lett.* **91**, 016802 (2003).
8. Hofmann, A. et al. Measuring the degeneracy of discrete energy levels using a GaAs/AlGaAs quantum dot. *Phys. Rev. Lett.* **117**, 206803 (2016).
9. Cooper, N. R. & Stern, A. Observable bulk signatures of non-Abelian quantum Hall states. *Phys. Rev. Lett.* **102**, 176807 (2009).
10. Ben-Shach, G., Laumann, C. R., Neder, I., Yacoby, A. & Halperin, B. I. Detecting non-Abelian anyons by charging spectroscopy. *Phys. Rev. Lett.* **110**, 106805 (2013).
11. Smirnov, S. Majorana tunneling entropy. *Phys. Rev. B* **92**, 195312 (2015).
12. Hou, C.-Y., Shtengel, K., Refael, G. & Goldbart, P. M. Ettingshausen effect due to Majorana modes. *New J. Phys.* **14**, 105005 (2012).
13. Alkurtass, B. et al. Entanglement structure of the two-channel Kondo model. *Phys. Rev. B* **93**, 081106 (2016).
14. Elzerman, J. M. et al. Single-shot read-out of an individual electron spin in a quantum dot. *Nature* **430**, 431–435 (2004).
15. Ono, K. & Tarucha, S. Nuclear-spin-induced oscillatory current in spin-blockaded quantum dots. *Phys. Rev. Lett.* **92**, 256803 (2004).
16. Landau, L. D. & Lifshitz, E. M. *Statistical Physics* 3rd edn 158–190 (Butterworth-Heinemann, Oxford, 1980).
17. Venkatachalam, V., Yacoby, A., Pfeiffer, L. & West, K. Local charge of the $\nu=5/2$ fractional quantum Hall state. *Nature* **469**, 185–188 (2011).
18. Field, M. et al. Measurements of Coulomb blockade with a noninvasive voltage probe. *Phys. Rev. Lett.* **70**, 1311–1314 (1993).
19. Staring, A. A. M. et al. Coulomb-blockade oscillations in the thermopower of a quantum dot. *EPL* **22**, 57 (1993).
20. Thierschmann, H. et al. Three-terminal energy harvester with coupled quantum dots. *Nat. Nanotech* **10**, 854–858 (2015).
21. Beenakker, C. W. J. Theory of Coulomb-blockade oscillations in the conductance of a quantum dot. *Phys. Rev. B* **44**, 1646–1656 (1991).
22. Gustavsson, S. et al. Electron counting in quantum dots. *Surf. Sci. Rep.* **64**, 191–232 (2009).
23. Cockins, L. et al. Energy levels of few-electron quantum dots imaged and characterized by atomic force microscopy. *Proc. Natl Acad. Sci. USA* **107**, 9496–9501 (2010).
24. Bennett, S. D., Cockins, L., Miyahara, Y., Grütter, P. & Clerk, A. A. Strong electromechanical coupling of an atomic force microscope cantilever to a quantum dot. *Phys. Rev. Lett.* **104**, 017203 (2010).
25. Beckel, A. et al. Asymmetry of charge relaxation times in quantum dots: The influence of degeneracy. *EPL* **106**, 47002 (2014).
26. Cronenwett, S. M., Oosterkamp, T. H. & Kouwenhoven, L. P. A tunable Kondo effect in quantum dots. *Science* **281**, 540–544 (1998).
27. Hanson, R. et al. Zeeman energy and spin relaxation in a one-electron quantum dot. *Phys. Rev. Lett.* **91**, 196802 (2003).
28. Zumbühl, D. M., Marcus, C. M., Hanson, M. P. & Gossard, A. C. Cotunneling spectroscopy in few-electron quantum dots. *Phys. Rev. Lett.* **93**, 256801 (2004).
29. Szafran, B., Peeters, F. M., Bednarek, S. & Adamowski, J. In-plane magnetic-field-induced Wigner crystallization in a two-electron quantum dot. *Phys. Rev. B* **70**, 235335 (2004).
30. Mittal, A., Wheeler, R. G., Keller, M. W., Prober, D. E. & Sacks, R. N. Electron–phonon scattering rates in GaAs/AlGaAs 2DEG samples below 0.5 K. *Surf. Sci.* **361–362**, 537–541 (1996).

## Acknowledgements

The authors acknowledge J. Martinis for a helpful discussion on the interpretation of our measurements. N.H., C.O., S.L., M.S. and J.F. were supported by the Canada Foundation for Innovation, the National Science and Engineering Research Council, CIFAR and SBQMI. S.F., G.C.G. and M.M. were supported by the US DOE Office of Basic Energy Sciences, Division of Materials Sciences and Engineering award no. DE-SC0006671, with additional support from Nokia Bell Laboratories for the MBE facility gratefully acknowledged.

## Author contributions

N.H. and C.O. fabricated the mesoscopic device. GaAs heterostructures and their characterization were provided by S.F., G.C.G. and M.M. S.L. and M.S. worked on early versions of the experiment and provided helpful discussion. N.H. performed measurements and analysed data. The manuscript was written by N.H. and J.F. with additional feedback from all authors.

## Competing interests

The authors declare no competing interests.

## Additional information



**Correspondence and requests for materials** should be addressed to N.H. or J.F.

## Methods

The device was built on a AlGaAs/GaAs heterostructure, hosting a 2DEG with density and mobility at 300 mK of $2.42\times10^{11}\,\mathrm{cm}^{-2}$ and $2.56\times10^{6}\,\mathrm{cm}^{2}/(\mathrm{Vs})$ respectively, determined in a separate measurement. Mesas and NiAuGe ohmic contacts to the 2DEG were defined by standard photolithography techniques, followed by atomic layer deposition of 10 nm $HfO_2$ to improve the gating stability in the device. Fine gate structures, shown in Fig. 1a, were defined by electron beam lithography and deposition of 3 nm Ti/18 nm Au.

The measurement was carried out in a dilution refrigerator with a two-axis magnet. The 2DEG was aligned parallel to the main axis with the second axis used to compensate for sample misalignment. In practice, out-of-plane fields up to 100 mT showed no effect on our data. A retuning of the quantum dot gates was necessary to capture the bias spectroscopy data in Figs. 3d,e and 4e,f. The rightmost gate (Fig. 1a) on the quantum dot was used to tune between the one- and two-lead configurations, for the entropy and bias spectroscopy measurements, respectively. This tuning had a significant effect on the shape of the potential well, accounting for variations in parameters such as $g$ and $\Delta_{ST}$ between the two measurement configurations. Charge sensor conductance was measured using a d.c. voltage bias of 200–350 μV; we find that Joule heating through the sensor does not affect our reservoir temperatures up to $V_{\mathrm{sens}}\sim500\,\mu\mathrm{V}$. The d.c. current ($I_{\mathrm{sens}}$) was measured using an analogue–digital convertor while the a.c. current ($\delta I_{\mathrm{sens}}$) was measured using a lock-in amplifier. The d.c. conductance reported here is $G_{\mathrm{sens}}=I_{\mathrm{sens}}/V_{\mathrm{sens}}$ while the oscillations are defined as $\delta G_{\mathrm{sens}}=(\delta I_{\mathrm{sens}})/V_{\mathrm{sens}}$.

The temperature of the reservoir was raised above the substrate temperature using $I_{\mathrm{heat}}$ at a.c. or d.c., with the QPC heater set by gate voltages to 20 kΩ. Applying a.c. current at $f_{\mathrm{heat}}=48.7\,\mathrm{Hz}$ yields an oscillating Joule power, $P_{\mathrm{heat}}=I_{\mathrm{heat}}^{2}R_{\mathrm{QPC}}$. To leading order, this gives oscillations in temperature, and therefore $\delta G_{\mathrm{sens}}$, at $2f_{\mathrm{heat}}$. These are captured by the lock-in amplifier at the second harmonic of $I_{\mathrm{heat}}$. Except where noted, measurements of $\Delta S$ were made at $\delta T\sim50\,\mathrm{mK}$, although the error bars in Fig. 2 demonstrate that the measurements would have been just as accurate with $\delta T$ set to 30 mK.

**Code availability.** The github repository (https://github.com/nikhartman/spin_entropy) contains all code necessary to complete the analysis and create each of the figures in this manuscript.

**Data availability.** Data generated for, and analysed in, this study are available at https://github.com/nikhartman/spin_entropy.